Implementation of Acceleration Source Term in FUN3D

Nash'at N. Ahmad*, Jan-Renee Carlson†, Craig Streett‡, Robert T. Biedron§
NASA Langley Research Center, Hampton, Virginia, 23681

Implementation of the acceleration source term in FUN3D is described. The method is evaluated using analytical and idealized test cases in two and three dimensions. It is also compared with results obtained from the moving mesh and six-degree-of-freedom simulations. The method shows promise in simulating the flight of accelerating vehicles as they make their ascent through varying reference conditions.

I. Introduction

Accelerating flows are of interest in many practical engineering applications. Earlier studies on the subject used simple geometries for incompressible flows at low Reynolds number.[1–2] It was found in experiments and numerical simulations of accelerating flow past an airfoil at high angles of attack that the duration of the applied acceleration was more of a contributing factor in inducing flow separation than the magnitude of the applied acceleration.[1] Badr et al.[2] conducted simulations of flow around an accelerating cylinder, and showed the formation of corotating vortices in the wake region.

Inoue et al. simulated the breakup of the bow shock due to linear acceleration of a projectile in supersonic flight.[3] Recent experiments and numerical studies in ballistics have shown that the deceleration experienced by a projectile can result in an increase in the shock stand-off distance.[4–5] Studies on acceleration effects on missiles showed lower drag in the transonic region for accelerating vehicles.[6–7] Acceleration effects are also important in the sonic boom generation, which remains an impediment to future supersonic air transportation systems. As the aircraft accelerates through the transonic range to cruise speed, it causes the focusing of the shock waves, which can generate unacceptable levels of overpressure at the ground.[8–10] Blumrich et al.[10] analyzed one year's worth of flight and meteorological data for Concorde transatlantic flights between New York and Paris. They found that the caustics occurred over the English Channel during the acceleration phase for flights from Paris to New York.

The target application of this study is the characterization of the buffet environment of launch vehicles. As the flight vehicle ascends along its trajectory, it is subjected to different external forces due to turbulence (atmospheric and flow-induced), transonic shocks, and disturbances caused by the plumes from the main engines. Identification of the conditions and the regions in which the induced pressure perturbations can undermine the structural integrity of the vehicle is a vital step in the design cycle. Traditionally this task has been accomplished in wind tunnel tests[11–14] because of the prohibitive cost associated with running unsteady Computational Fluid Dynamics (CFD) simulations. With the increase in available computational resources, it is now becoming feasible to use CFD for simulating time-dependent flows around complex configurations for both analysis and design.[15–16]

Recently Alter et al.[15] conducted simulations of transonic flowfields around the Space Launch System (SLS) configuration to establish best CFD practices. This included grid convergence, computational domain size, and time-step sensitivity studies. They also evaluated the simulation results using measurements from NASA Ames' 11-Foot Transonic Wind Tunnel with good agreement between the simulated and the measured data. Engblom[16] used CFD simulations to identify the cause of large vibrations experienced by the Titan IVB launch vehicle during transonic flight.

Past analyses on the characterization of the buffet environment have been conducted for fixed reference conditions. This paper presents a simple methodology for simulating the flow around vehicles that are accelerating through varying reference conditions by adding the acceleration as a source term. Unlike the more commonly used moving mesh method, the mesh in this case remains stationary and instead, the flow is accelerated. The main objective of this study was to validate the implementation of the acceleration source method in the Fully Unstructured Navier-Stokes 3D (FUN3D) code. The results of this evaluation are presented in this paper.

---

* Research Scientist, Computational Aerosciences Branch. Senior Member, AIAA.
† Research Scientist, Computational Aerosciences Branch. Associate Fellow, AIAA.
‡ Senior Research Scientist, Computational Aerosciences Branch.
§ Research Scientist, Computational Aerosciences Branch.

II. The Fully Unstructured Navier-Stokes 3D (FUN3D) Software

The Fully Unstructured Navier-Stokes 3D (FUN3D)[17–19] code has been used to solve complex flow problems ranging from hypersonics[20] to aeroacoustics[21] (`https://fun3d.larc.nasa.gov`). FUN3D has extensive fluid-structure interaction capabilities for aeroelastic[22] and rotorcraft analysis.[23] The flow solver is based on a node-centered, finite-volume scheme designed to compute both compressible and incompressible flows on grids with different types of elements (tetrahedron, pyramid, prism, and hexahedron elements). Several schemes are available for computing the convective fluxes. Computation of viscous fluxes on tetrahedral meshes is based on the Green-Gauss theorem and on nontetrahedral grids, an edge-derivative augmentation is employed to avoid odd-even decoupling. A number of turbulence models (`https://turbmodels.larc.nasa.gov`)[24] have been implemented in the code that range from single equation models to hybrid Reynolds-averaged Navier-Stokes/Large Eddy Simulation (RANS/LES) capability. Time integration is implemented as a series of backward-Euler schemes with local time-stepping to accelerate convergence within each time step.[25]

A. Acceleration Source Term

Consider the Euler part of the compressible Navier-Stokes Equations, which can be written in a linearly accelerating reference frame as:[5]

$$\frac{\partial \rho}{\partial t} + \nabla \cdot \left(\rho \mathbf{v} \right) = 0 \,, \tag{1}$$

$$\frac{\partial \rho \mathbf{v}}{\partial t} + \nabla \cdot \left(\rho \mathbf{v}\mathbf{v} \right) + \nabla p = -\rho \mathbf{a} \,, \tag{2}$$

$$\frac{\partial \rho E}{\partial t} + \nabla \cdot \left[\left(\rho E + p \right) \mathbf{v} \right] = -\rho \mathbf{v} \cdot \mathbf{a} \,, \tag{3}$$

where ρ is the fluid density, $\mathbf{v}$ is the velocity vector relative to the accelerating frame, p is pressure, $\mathbf{a}$ is the acceleration vector relative to an inertial reference frame, and E is the total energy. In the current implementation, the acceleration source term in Eqs. (2)–(3) is added to the right hand side at each time step. The farfield boundary conditions are updated at each time step based on the Mach profile, and the adiabatic wall temperature is reset based on the updated Mach number.

FUN3D implements Eqs. (1)–(3) in the nondimensional form. Within FUN3D, acceleration is calculated in each time step from the prescribed Mach profile, and then nondimensionalized,

$$\mathbf{a}^* = \frac{\mathbf{a} L}{c^2}, \tag{4}$$

where $\mathbf{a}^*$ is the nondimensional acceleration, L is the characteristic length, c is the speed of sound and $\mathbf{a}$ is the dimensional acceleration obtained from the user-specified Mach profile.

B. Moving Mesh

Several methods of moving the geometries are implemented in FUN3D, including coupling with structural models, prescribed motion,[25–26] and coupling with a six-degree-of-freedom (6-DOF)[27–28] model. FUN3D can simulate the flows around geometries that are undergoing rigid-body motion, deformation, or both at the same time. Translations and rotations are implemented using the moving mesh method in which the entire mesh moves according to a prescribed trajectory. Geometries undergoing relatively small deformations are modeled with equations that are analogous to linear elasticity. Large relative motions are handled using overset grids.

The simple test cases (Section III.C and III.D) for validating the acceleration source term method in this study, use the baseline moving mesh method, in which the mesh is translated using a prescribed trajectory. The sphere in freefall test case described in Section III.B is simulated using the 6-DOF library.

III. Results

A. Transport of Density Distribution

Deiterding[29] has suggested a simple test case with an analytical solution for evaluating numerical schemes for the Euler equations with the acceleration source term. In the presence of an acceleration source term, the Euler equations in two dimensions can be reduced to a single transport equation for density as follows:

$$u(x,z,t)=u_0;\quad w(x,z,t)=w_0-at;\quad p(x,z,t)=p_0;\quad \rho(x,z,t)=\rho_0\left(x-u_0t,\ z-w_0t+\frac{1}{2}at^2\right), \tag{5}$$

The computational domain in this case was defined as $(x,z)\in[0,2]\times[0,2]$ with $t\in[0,0.5]$. The mesh size was 80×80 cells (quad cells). A nondimensional time step of 0.002 was used and the number of time subiterations per time step was set to 10. The simulation was marched in time using a second-order backward difference scheme.[25] Periodic boundary conditions were used in both *x* and *z* directions.

The transport of density distribution is given by:

$$x_c(t)=x_0+u_0t;\qquad z_c(t)=z_0+w_0t-\frac{1}{2}at^2, \tag{6}$$

The initial density distribution is defined as follows:

$$\rho(r)=\begin{cases}\rho_1+\rho_2\left[\sin\left(\dfrac{r}{R}\pi+\dfrac{\pi}{2}\right)+1\right] & if\ 0\le r<R\\ \rho_1 & if\ r\ge R\end{cases}, \tag{7}$$

where, $r(x,z,t)=\sqrt{\left(x-x_c(t)\right)^2+\left(z-z_c(t)\right)^2}$, and $R=0.5$, $\rho_1=1$, $\rho_2=0.05$, $x_0=0.75$, $z_0=0.75$, $u_0=1$, $w_0=1.25$, $p_0=1$, $a=1$, and $\gamma=1.4$.

The density distribution at time = 0.5 is shown in Figure 1 (left panel). The computed results using Nishikawa and Liu's low dissipation Roe scheme[30] are compared with the analytical solution in Figure 1 (right panel). Flux limiting was not used in this calculation. The computed results are in good agreement with the analytical solution.

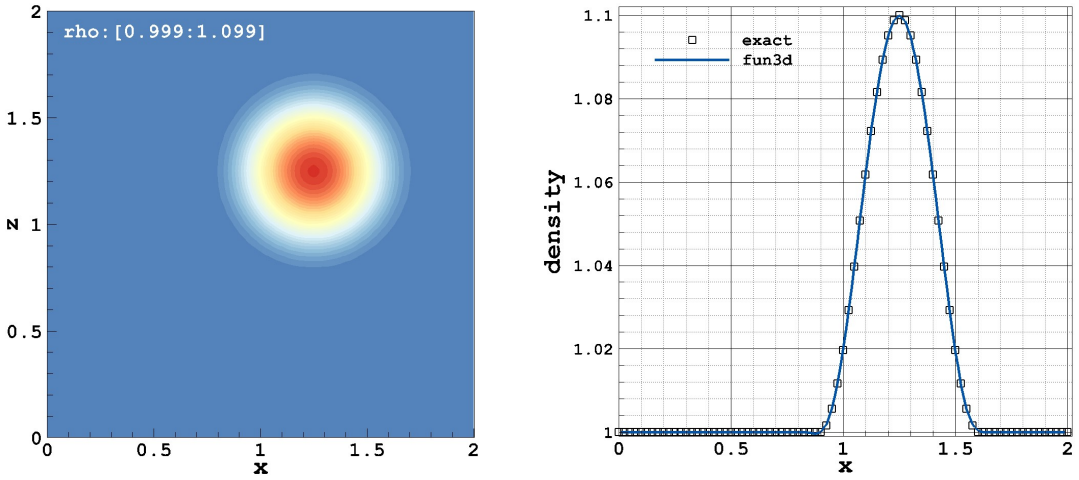

Figure 1. Transport of Density Distribution. The computed density distribution at time = 0.5 is shown in the left panel and the comparison of the computed solution with the analytical solution along the mesh diagonal at time = 0.5 is shown in the right panel.

B. Sphere in Freefall

Simulations of a sphere in freefall using the acceleration source term are compared with 6-DOF calculations in this section. A sphere of unit diameter was bounded by the farfield at a radius of 15 units from the center of the sphere. Two inviscid grids of medium and fine resolution were generated with 848,148 and 12,092,376 nodes, respectively.[31] In the first step, a steady state solution was obtained with the reference Mach number set to 0.2. The Roe[32] scheme with no flux limiting was used for this run. Figure 2 shows the grids and the steady state solution on the fine mesh.

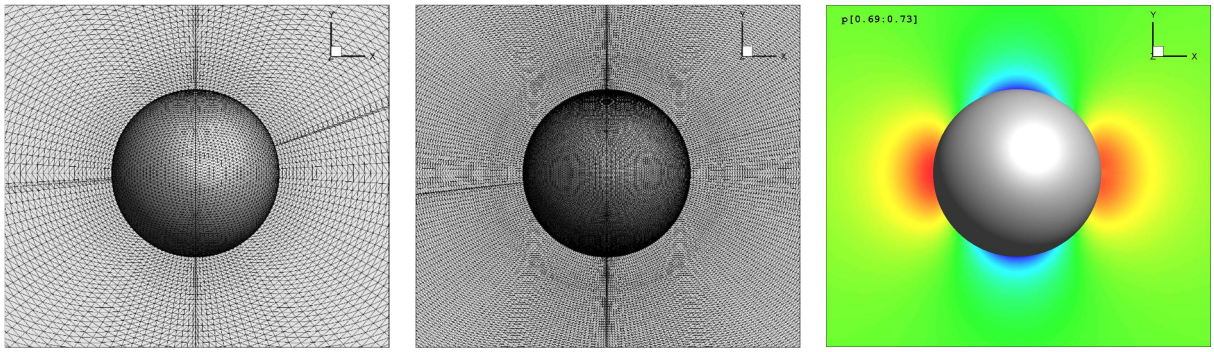

Figure 2. Sphere in Freefall. Medium grid (left), fine grid (center), and the steady (inviscid) solution on the fine mesh (right).

The acceleration runs were started from the steady state solutions. The gravitational acceleration of the sphere with unit mass in the 6-DOF simulation was set to 9.81 m/s^2 in the negative x direction and the freestream speed of sound was set to 340.46 m/s. A constant acceleration of 9.81 m/s^2 in the negative x direction relative to the inertial frame was imposed in the acceleration source simulations. The simulations were run for 100 time steps using a non-dimensional time step of 0.05 and 50 time subiterations per time step. The simulation was marched in time using a second-order backward difference scheme.[25] Both methods converge to machine zero in each time step. The Roe solver[32] with no flux limiting was used in the acceleration runs. The reference Mach number was fixed at 0.2. Farfield boundary conditions were updated in the acceleration source term run at each time step.

Figure 3 shows the comparison of pressure contours obtained using the acceleration source term method and the 6-DOF simulations on the medium and fine grids. The results obtained from the two methods are almost identical. At the final time step, the drag coefficients calculated on the medium grid were 0.44139190×10^{-2} and 0.44139199×10^{-2} for the 6-DOF and the acceleration source simulations, respectively. Simulations were conducted on the fine mesh to see if the grid refinement would give a closer comparison. On the fine mesh, the C_D was $0.1359086018\times10^{-2}$ for both the 6-DOF and the acceleration source simulations.

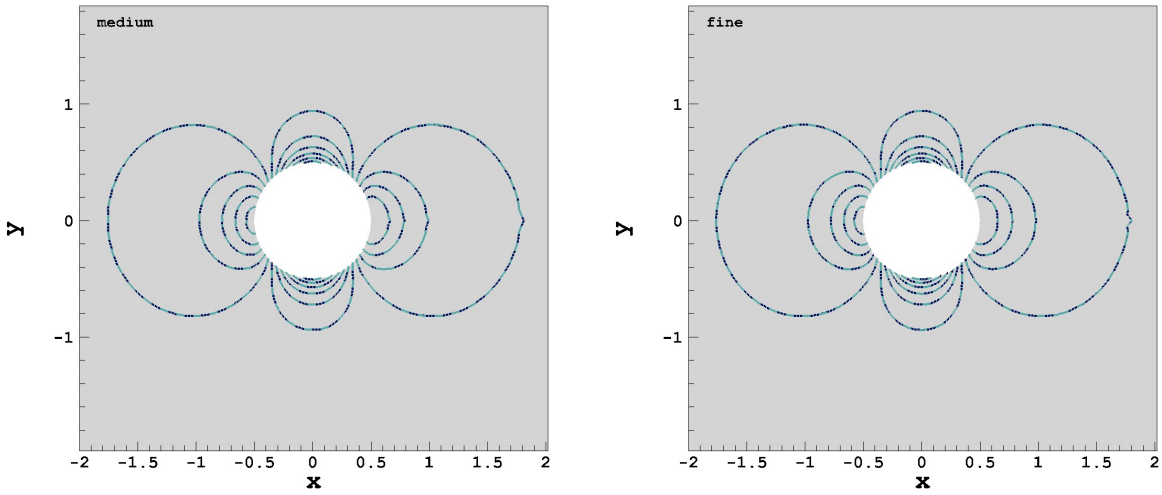

Figure 3. Sphere in Freefall. Comparison of the acceleration source term (solid line) and 6-DOF (dashed line) simulations on the medium (left) and fine (right) grids. Pressure contours after 100 time steps are shown in the figure.

C. Moving Mesh vs. Acceleration Source Term

A simple geometry with an ogive nose and a bluff tail was used to compare the solutions obtained using the acceleration source term with the moving mesh method. The grid generated for this case was relatively coarse with approximately 2.5 million nodes. The method for initializing the simulations was similar to what is described in Alter et al.[15] A set of simulations was first run to allow the transients to leave the domain and allow the flow to reach a quasisteady state. The initial flow was uniform throughout the domain in these runs, except for the region around the geometry, where it was set to zero in order to accelerate convergence. Once the flow field was established, the restart file was used to initialize both the moving mesh and the acceleration source term runs. The Mach number was gradually increased from 0.7 to 0.95 in the first 10,000 time steps according to the prescribed profile shown in Figure 4 (left); after which, it was held constant at 0.95. The Reynolds number was set to 3×10^6 based on the unit reference length (diameter of the body). The reference temperature, T_{ref} was 534.7°R, and the angle of attack, α was 4°. The computational domain was defined as $(x,y,z)\in[-49.6,80.4]\times[-49.8,49.8]\times[-49.8,49.8]$ with $t\in[0,600]$. The characteristic length, L based on the base diameter of the geometry was set to 1.

Nishikawa and Liu's low-dissipation Roe scheme[30] with the van Albada limiter[33] was used for inviscid flux construction and the Delayed Detached Eddy Simulation (DDES)[34] with modifications[35] was used for turbulence calculations. The simulation was marched in time using a second-order backward difference scheme[25] for 12,000 time steps with a nondimensional time-step of 0.05 and 10 time subiterations within each time step. The farfield boundary conditions and the reference Mach number were updated at each time step. The adiabatic wall temperature was also reset at each time step based on the updated Mach number. The reference Mach number was not updated in the moving mesh simulation. There was also a slight difference in the farfield boundary conditions for the two methods. Node-based and edge-based Riemann conditions at the farfield were used in the moving mesh and the acceleration source simulations, respectively.

Figure 4 (left panel) shows the input Mach profile, and the right panel shows the comparison of Mach profiles along the stagnation line at different time steps for the moving mesh and the acceleration source simulations. Mach profiles from both simulations are almost identical. Figures 5 and 6 show the comparison of Mach contours for the source term and moving mesh simulations at 6,000 and 12,000 time steps, respectively. The two solutions are in good agreement except for some differences in the wake region. These differences can be due to slight differences in the boundary conditions. The field maximums for the two methods are slightly different for the two methods. For example, the maximum Mach number was 1.51 for the acceleration source case at the final iteration compared to 1.49 in the moving mesh method. The predictions of the shock locations are similar for the two methods.

Results obtained using Nishikawa and Liu's low-dissipation Roe scheme[30] were also compared with Edward's low dissipation scheme[36] for the acceleration source case. The two schemes gave similar results with the exception of small differences in the wake region.

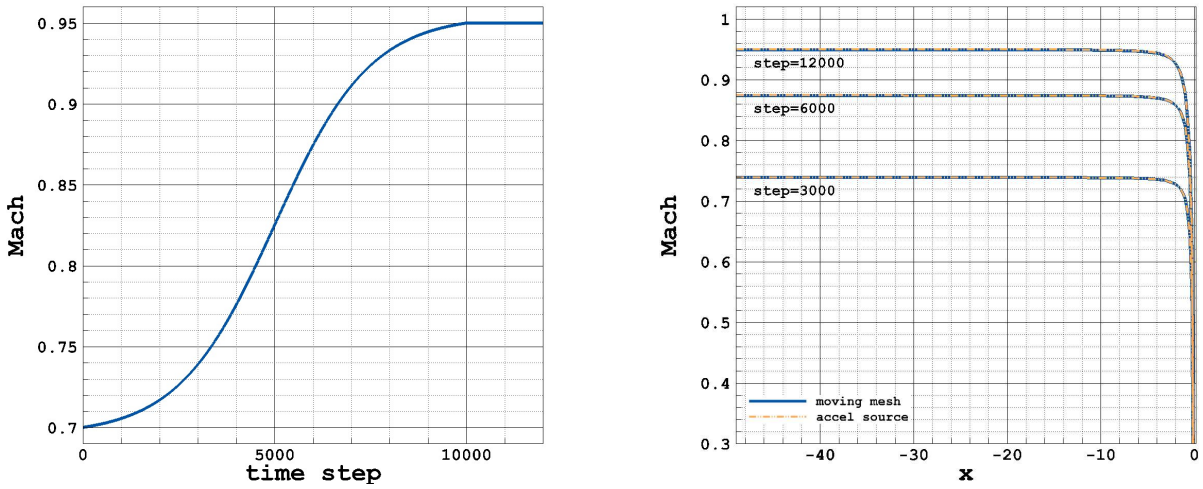

Figure 4. Left panel shows the input Mach profile – the Mach number is increased from 0.7 to 0.95 in the first 10,000 time steps, and then held constant at 0.95 in the last 2,000 time steps. Right panel shows the comparison of the Mach profiles along the stagnation line at different time steps into the simulation. The moving mesh data are shown by the solid line and the acceleration source simulation data are shown by the dash-dotted line.

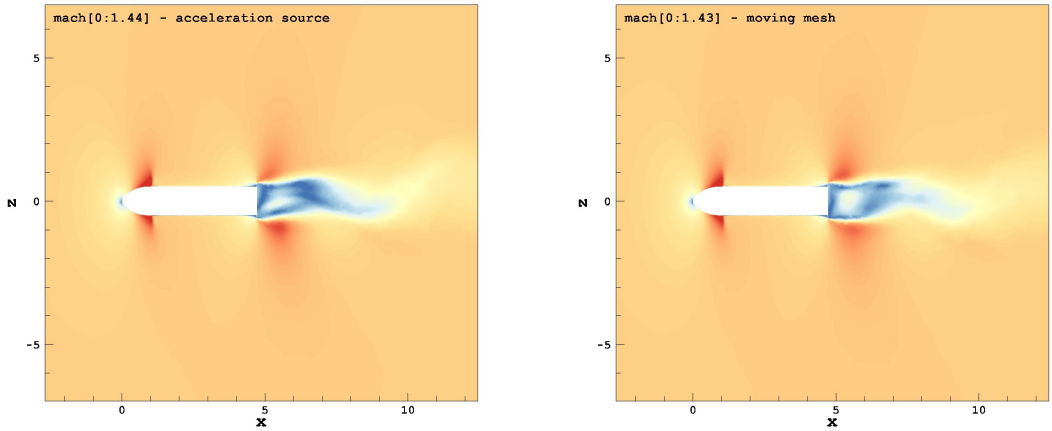

Figure 5. Comparison of results obtained using the acceleration source term (left panel) with the moving mesh simulation (right panel). The figure shows Mach contours in the *xz* plane for $y = 0$ at time step = 6000 into the simulation. M = 0.7–0.95, Re = 3×10^6, $\alpha = 4°$.

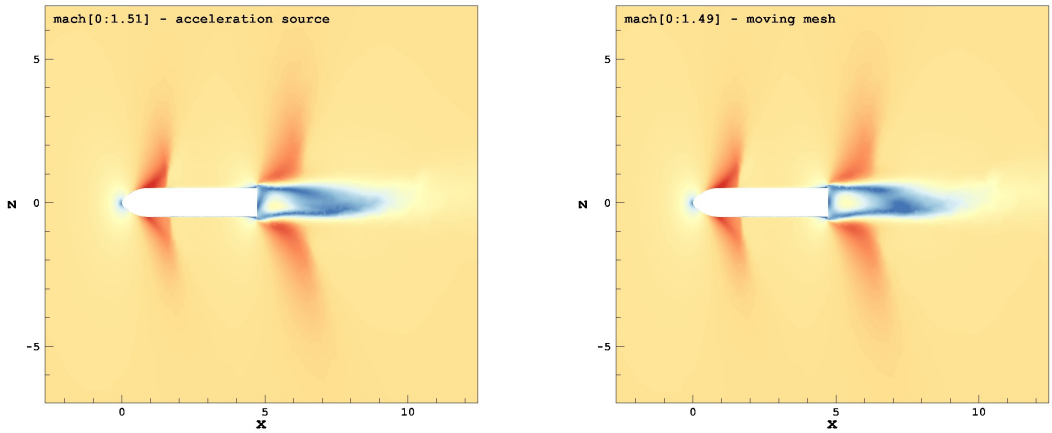

Figure 6. Comparison of results obtained using the acceleration source term (left panel) with the moving mesh simulation (right panel). The figure shows Mach contours in the *xz* plane for $y = 0$ at the final time step of the simulation. M = 0.7–0.95, Re = 3×10^6, $\alpha = 4°$.

D. Coe-Nute Sounding Rocket

A comparison of the acceleration source and the moving mesh methods using the Coe-Nute[37] sounding rocket is presented in this section. The simulation initialization was similar to the method described in Section C. In this case, the flow was accelerated from M = 0.75 to M = 1.06. The Reynolds number was set to 3.9 million based on the unit reference length (diameter of the vehicle base), and the angle of attack was zero. The computational domain was defined as $(x, y, z) \in [-82.8, 83.8] \times [-83, 83] \times [-83, 83]$ with $t \in [0, 1200]$. The mesh had approximately 17 million nodes. The characteristic length was 1 based on the diameter of the vehicle base, the nondimensional time step was 0.04, and the number of time subiterations within each time step was set to 10. The simulation was run for 30,000 time steps. The simulation was marched in time using a second-order backward difference scheme.[25] Nishikawa and Liu's low-dissipation Roe scheme[30] was used with the van Albada limiter.[33] DDES[34] with modifications[35] was used for turbulence calculations. The simulation took approximately 72 hours to run using 1024 processes on NASA Langley's K-cluster.

In Figure 7, the left panel shows the input Mach profile, and the right panel shows the comparison of Mach profiles along the stagnation line at different time steps for the moving mesh and the acceleration source simulations. Mach profiles from both simulations are almost identical. Figure 8 shows the comparison of Mach contours for the source term and moving mesh simulations at 15,000 and 30,000 time steps. As in the previous case (ogive geometry), the two solutions compare well with each other. The small differences seen in the solutions are likely due to differences in the farfield boundary conditions.

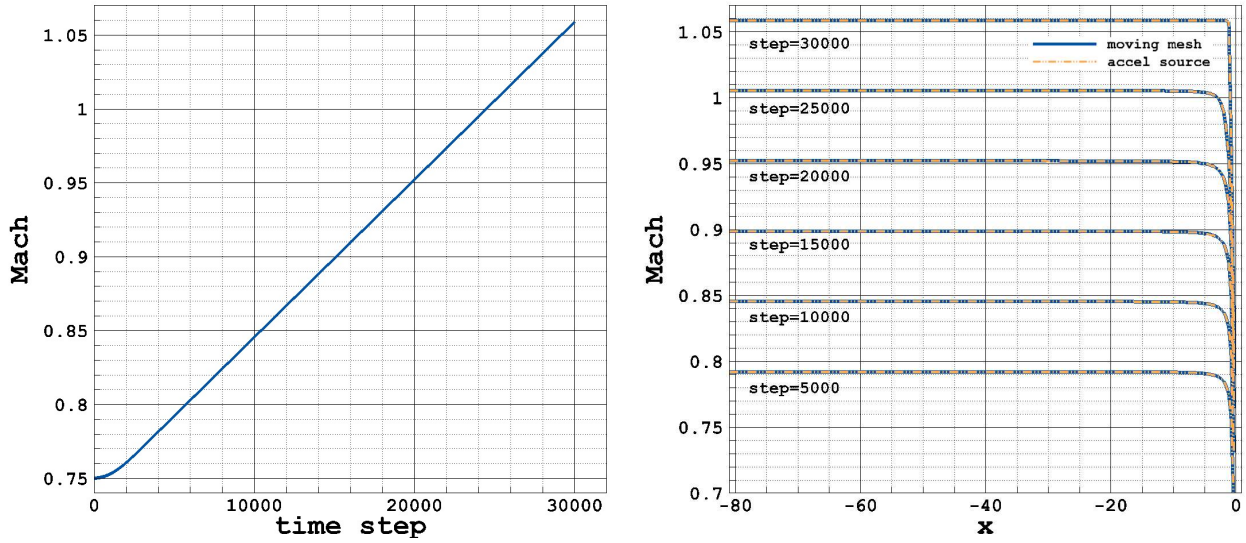

Figure 7. Coe-Nute Launch Vehicle. Left panel shows the input Mach profile. Right panel shows the comparison of the Mach profiles along the stagnation line at different time steps into the simulation. The moving mesh data are shown by the solid line and the acceleration source simulation data are shown by the dash-dotted line.

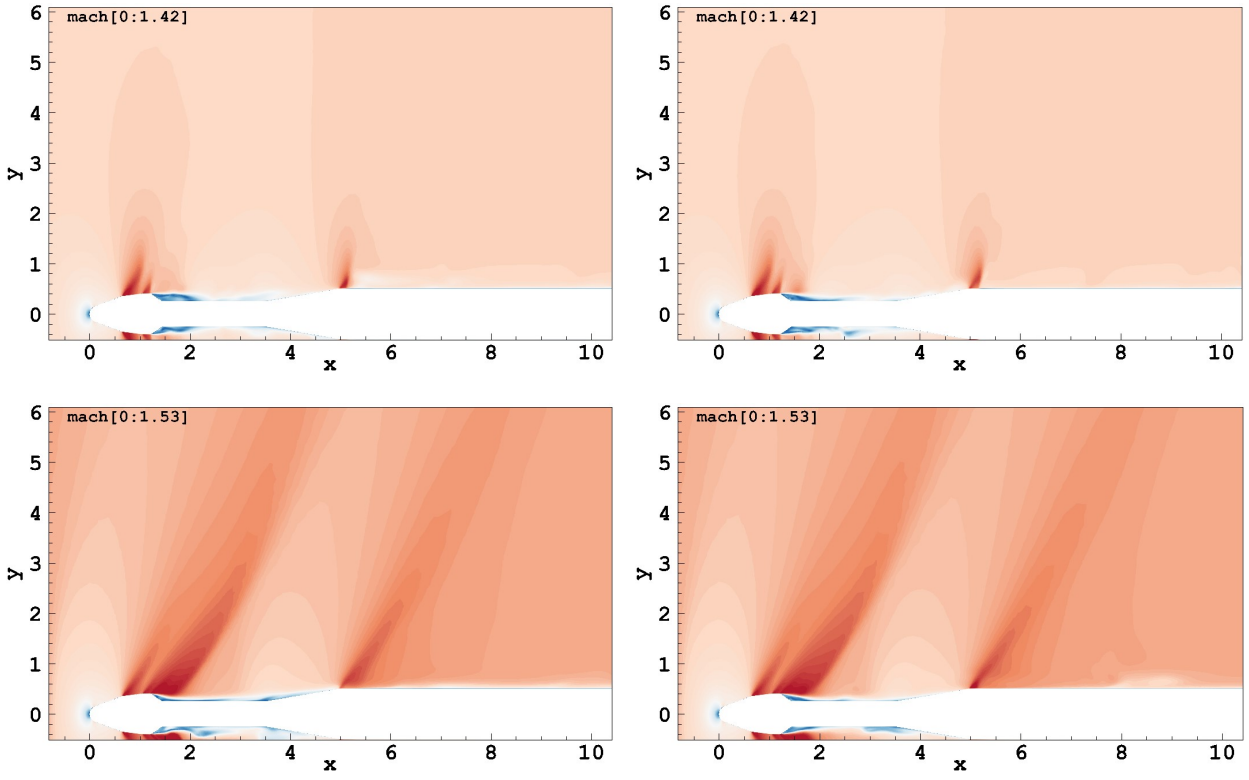

Figure 8. Coe-Nute Launch Vehicle. Mach contours in the *xy* plane for $z = 0$ at the 15,000 time step are shown in the top row and at the 30,000 time step are shown in the bottom row. The acceleration source term, and the moving mesh solutions are in the left and the right columns, respectively. The simulation was run for 30,000 time steps with a nondimensional time step of 0.04. The mesh had ~17 million nodes. M = 0.75–1.06, Re = 3.9×10^6, $\alpha = 0°$. The total length of the vehicle is 11.65 units.

Figure 9 shows the comparison of the pressure contours for the source term and moving mesh simulations at different time steps. The solutions obtained from the two methods are in good agreement with each other.

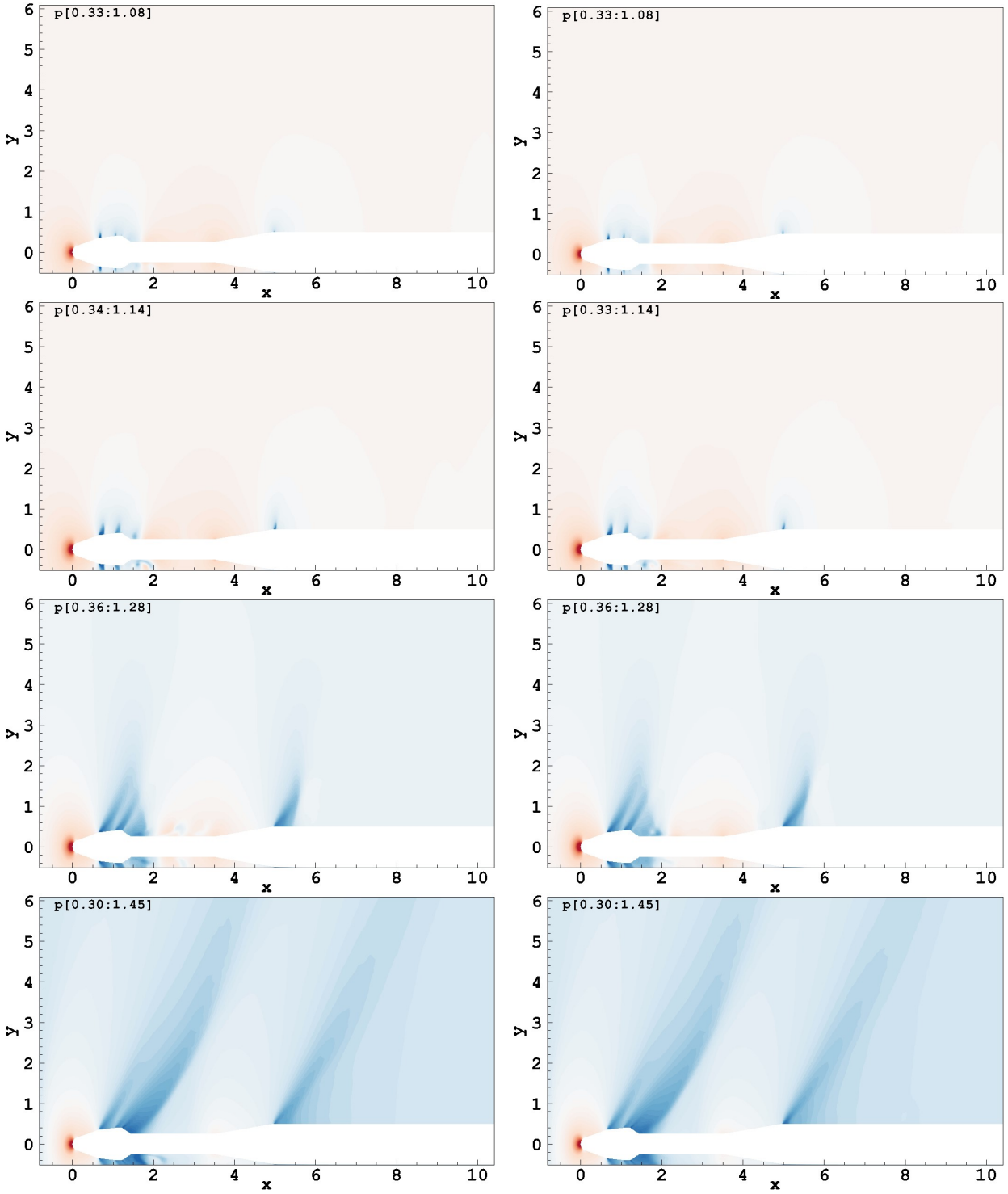

Figure 9. Coe-Nute Launch Vehicle. Pressure contours in the *xy* plane for $z = 0$, from top to bottom row at 5,000, 10,000, 20,000, and 30,000 time steps. The acceleration source term, and the moving mesh solutions are in the left and the right columns, respectively. M = 0.75–1.06, Re = 3.9×10^6, $\alpha = 0°$. The total length of the vehicle is 11.65 units.

E. Variable Reference Conditions

A set of runs was performed using the ogive geometry to assess the feasibility of changing the reference conditions during the simulation. As in the earlier runs, first the initial flow fields were generated to eliminate transients for the lower and upper bounds, 1) M = 0.4, Re = 2×10^6; and 2) M = 0.8, Re = 4×10^6. The lower bound flow field was used as the initial state for the acceleration simulation. The angle of attack, α was set to 4°.

Edward's low dissipation scheme[36] was used in these simulations with the van Albada limiter.[33] DDES[34] with Vatsa and Lockard modifications[35] was used for turbulence calculations. The simulations were run for 15,000 time steps using a nondimensional time step of 0.05. The simulation was marched in time using a second-order backward difference scheme.[25] The reference conditions were updated in the acceleration source term simulation at each time step. Along with the boundary conditions, other relevant parameters such as the wall temperature were also updated.

Figure 10 shows the comparison of Mach contours for the source term simulation with the lower and upper bound runs at the final time step. The final flow field obtained from the source term simulation with varying reference conditions compares well with the upper bound flow field.

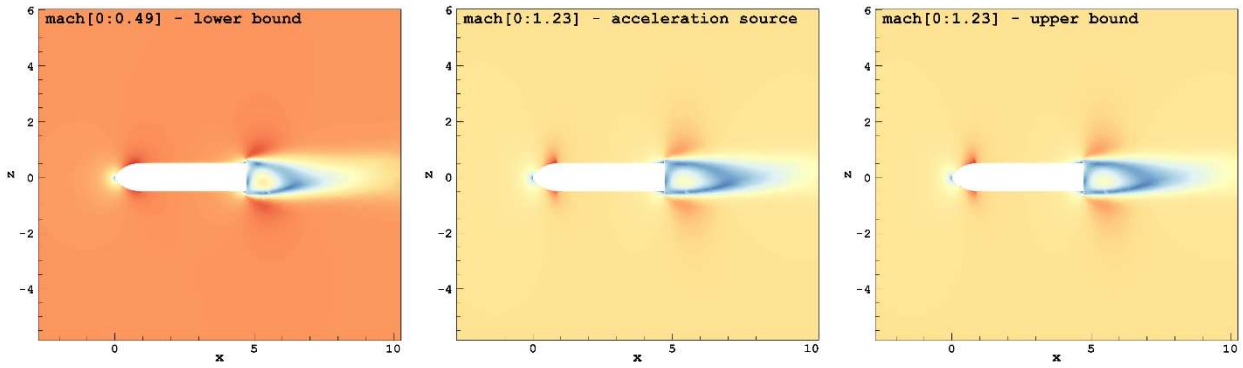

Figure 10. Mach contours in the *xz* plane for $y = 0$ at the final time for the three simulations. M = 0.4 and Re = 2×10^6 (left panel). M = 0.8 and Re = 4×10^6 (right panel). The center panel shows the solution for flow, which started with reference conditions of M = 0.4 and Re = 2×10^6 and was linearly accelerated to the final reference conditions of M = 0.8 and Re = 4×10^6.

IV. Summary

The capability of simulating flow around accelerating vehicles using a source term was implemented in FUN3D and evaluated using analytical and idealized test cases. The method compared well with the moving mesh and the 6-DOF methods implemented in FUN3D. A set of simulations was conducted to assess the feasibility of the method for variable reference conditions. For these idealized tests the method was bounded between the lower and upper limits of the specified reference conditions. The method is robust, efficient, easy to implement, and shows promise in simulating the flight of accelerating vehicles through varying atmospheric conditions with the use of static meshes.

Acknowledgement

This work supports the NASA Engineering and Safety Center (NESC) assessment of the Launch Vehicle Aerodynamic Buffet Flight Test. The simulations were run on the NASA Langley Research Center K-Cluster.

References

[1]Sengupta, T.K., Lim, T.T., Sajjan, S.V., Ganesh, S., Soria, J., "Accelerated flow past a symmetric aerofoil: experiments and computations," *Journal of Fluid Mechanics*, Vol. 591, 2007, pp. 255–288.

[2]Badr, H.M., Dennis, S.C.R., Kocabiyik, S., "Symmetrical flow past an accelerated circular cylinder," *Journal of Fluid Mechanics*, Vol. 308, 1996, pp. 97–110.

[3]Inoue, O., Sakai, T., Nishida, M., "Focusing shock waves generated by an accelerating projectile," *Fluid Dynamics Research*, Vol. 21, 1997, pp. 403–416.

[4]Starr, R.F., Bailey, A.B., Varner, M.O., "Shock Detachment Distance at Near Sonic Speeds," *AIAA Journal*, Vol. 14, 1976, pp. 537–539.

[5]Saito, T., Hatanaka, K., Yamashita, H., Ogawa, T., Obayashi, S., Takayama, K., "Shock stand-off distance of a solid sphere decelerating in transonic velocity range," *Shock Waves*, Vol. 21, 2011, pp. 483–489.

[6]Forsberg, K., Gledhill, I.M.A., Eliasson, P., Nordström, J., "Investigations of Acceleration Effects on Missile Aerodynamics using CFD," AIAA Paper 2003–4084.

[7]Gledhill, I.M.A., Forsberg, K., Eliasson, P., Bayloyi, J., Nordström, J., "Investigation of acceleration effects on missile aerodynamics using computational fluid dynamics," *Aerospace Science and Technology*, Vol. 13, 2009, pp. 197–203.

[8]Lilley, G.M., Westley, R., Yates, A.H., Busing, J.R., "Some Aspects of Noise from Supersonic Aircraft," *Journal of the Royal Aeronautical Society*, Vol. 57, 1953, pp. 396–414.

[9]Auger T., Coulouvrat, F., "Numerical Simulation of Sonic Boom Focusing," *AIAA Journal*, Vol. 40, 2002, pp. 1726–1734.

[10]Blumrich, R., Coulouvrat, F., Heimann, D. "Variability of focused sonic booms from accelerating supersonic aircraft in consideration of meteorological effects," *The Journal of the Acoustical Society of America*, Vol. 118, 2005, pp. 696–706.

[11]Sekula, M.K., Piatak, D.J., Rausch, R.D., "Analysis of Ares Crew Launch Vehicle Transonic Alternating Flow Phenomenon," *Journal of Spacecraft and Rockets*, Vol. 49, 2012, pp. 788–797.

[12]Piatak, D.J., Sekula, M.K., Rausch, R.D., "Ares Launch Vehicle Transonic Buffet Testing and Analysis Techniques," *Journal of Spacecraft and Rockets*, Vol. 49, 2012, pp. 798–807.

[13]Piatak, D.J., Sekula, M.K., Rausch, R.D., "Comparison of Ares I-X Wind-Tunnel-Derived Buffet Environment with Flight Data," *Journal of Spacecraft and Rockets*, Vol. 49, 2012, pp. 822–833.

[14]Panda, J., Roozeboom, N.H., Ross, J.C., "Wavenumber-Frequency Spectra on a Launch Vehicle Model Measured via Unsteady Pressure-Sensitive Paint," *AIAA Journal*, Vol. 57, 2019, pp. 1801–1817.

[15]Alter, S.J., Brauckmann, G.J., Kleb, B., Glass, C.E., Streett, C.L., Schuster, D.M., "Time-Accurate Unsteady Pressure Loads Simulated for the Space Launch System at Wind Tunnel Conditions," AIAA Paper 2015–3149.

[16]Engblom, W.A., "Numerical Simulation of Titan IVB Transonic Buffet Environment," *Journal of Spacecraft and Rockets*, Vol. 40, 2003, pp. 648–656.

[17]Anderson, W.K., Bonhaus, D.L., "An Implicit Upwind Algorithm for Computing Turbulent Flows on Unstructured Grids", *Computers and Fluids*, Vol. 23, 1994, pp. 1–22.

[18]Biedron, R.T., Carlson, J.-R., Derlaga, J.M., Gnoffo, P.A., Hammond, D.P., Jones, W.T., Kleb, B., Lee-Rausch, E.M., Nielsen, E.J., Park, M.A., Rumsey, C.L., Thomas, J.L., Thompson, K.B., Wood, W.A., "FUN3D Manual: 13.5," National Aeronautics and Space Administration, 2019, NASA/TM–2019–220271.

[19]NASA FUN3D CFD CODE, https://fun3d.larc.nasa.gov, Accessed: 2019-07-31.

[20]Gnoffo, P.A., Thompson, K., Korzun, A., "Tapping the Brake for Entry, Descent, and Landing," AIAA Paper 2016–4277.

[21]Vatsa, V.N., Khorrami, M.R., Lockard, D.P., "Aeroacoustic Simulations of a Nose Landing Gear with FUN3D: A Grid Refinement Study," AIAA Paper 2017–3009.

[22]Jacobson, K.E., Kiviaho, J.F., Smith, M.J., Kennedy, G.J., "An Aeroelastic Coupling Framework for Time-accurate Aeroelastic Analysis and Optimization," AIAA Paper 2018–0100.

[23]Wang, L., Diskin, B., Biedron, R.T., Nielsen, E.J., Sonneville, V., Bauchau, O.A., "High-Fidelity Multidisciplinary Sensitivity Analysis Framework for Multipoint Rotorcraft Optimization," AIAA Paper 2019–1699.

[24]Rumsey, C.L., "NASA Langley Research Center Turbulence Modeling Resource," https://turbmodels.larc.nasa.gov, Accessed: 2019-07-31.

[25]Biedron, R.T., Thomas, J.L., "Recent Enhancements to the FUN3D Flow Solver for Moving-Mesh Applications," AIAA Paper 2009–1360.

[26]Biedron, R. T., Vatsa, V. N., Atkins, H. L., "Simulation of Unsteady Flows Using an Unstructured Navier-Stokes Solver on Moving and Stationary Grids," AIAA Paper 2005–5093.

[27]Koomullil, R., Cheng, G., Soni, B., Noack, R., Prewitt, N., "Moving-body simulations using overset framework with rigid body dynamics," *Mathematics and Computers in Simulations*, Vol. 78, 2008, pp. 618–626.

[28]Koomullil, R., Prewitt, N., "A Library Based Approach for Rigid Body Dynamics Simulation," AIAA Paper 2007-4476.

[29]Deiterding, R., "Two-dimensional Euler equations with gravity." Technical Report NMWR–00–1. Institute of Mathematics, Technical University Cottbus, Germany. 2000.

[30]Nishikawa, H., Liu, Y., "Third-Order Edge-Based Scheme for Unsteady Problems," AIAA Paper 2018–4166.

[31]Nishikawa, H., "Making Your Own Mesh," Joint National Institute of Aerospace (NIA) and SU2 Foundation Users Workshop, August 2019, doi: 10.13140/RG.2.2.22227.53283.

[32]Roe, P.L., "Approximate Riemann Solvers, Parameter Vectors, and Difference Schemes," *Journal of Computational Physics*, Vol. 43, 1981, pp.357–372.

[33]van Albada, G.D., van Leer, B., Roberts, W.W., "A comparative study of computational methods in cosmic gas dynamics," *Astronomy and Astrophysics*, Vol. 108, 1982, pp. 76–84.

[34]Spalart, P.R., Deck, S., Shur, M.L., Squires, K.D., Strelets, M.K., Travin, A., "A new version of detached-eddy simulation, resistant to ambiguous grid densities," *Theoretical and Computational Fluid Dynamics*, Vol. 20, 2006, pp. 181–195.

[35]Vatsa, V.N., Lockard, D.P., "Assessment of Hybrid RANS/LES Turbulence Models for Aeroacoustics Applications," AIAA Paper 2014–4001.

[36]Edwards, J.R., "A Low-Diffusion Flux-Splitting Scheme for Navier-Stokes Calculations," *Computers and Fluids*, Vol. 26, 1997, pp. 635–659.

[37]Coe, C.F., Nute, J.B., "Steady and Fluctuating Pressures at Transonic Speeds on Hammerhead Launch Vehicles," National Aeronautics and Space Administration, 1962, NASA/TM–1962–X–778.